Synthesis, Characterization and Electronic Structure of the Novel 'Stellated' Octahedral Cluster $[Co_6(\mu_3\text{-}S)_7(\mu_3\text{-}H)(PEt_3)_6]^+$. Crystal and Molecular Structure of $[Co_6(\mu_3\text{-}S)_7(\mu_3\text{-}H)(PEt_3)_6]_{0.7}[Co_6(\mu_3\text{-}S)_8(PEt_3)_6]_{0.3}[BPh_4]$ *

Franco Cecconi,[a] Carlo A. Ghilardi,[a] Stefano Midollini,[a] Annabella Orlandini,[a] Piero Zanello,[b] Arnaldo Cinquantini,[b] Alessandro Bencini,[c] Myriam G. Uytterhoeven[c] and Gianluca Giorgi[d]

[a] *Istituto per lo Studio della Stereochimica ed Energetica dei Composti di Coordinazione, CNR, Via J. Nardi, 39, 50132 Firenze, Italy*

[b] *Dipartimento di Chimica, Università di Siena, Piano dei Mantellini, 44, 53100 Siena, Italy*

[c] *Dipartimento di Chimica, Università di Firenze, Via Maragliano, 75, Firenze, Italy*

[d] *Centro Interdipartimentale di Analisi e Determinazioni Strutturali, Università di Siena, Via P.A. Mattioli, 10, 53100 Siena, Italy*

Reaction of $Co(O_2CMe)_2\cdot 4H_2O$ with an excess of PEt_3 and H_2S afforded the novel diamagnetic octahedral cluster $[Co_6(\mu_3\text{-}S)_7(\mu_3\text{-}H)(PEt_3)_6]^+$ together with a minor amount of the known paramagnetic isostructural $[Co_6(\mu_3\text{-}S)_8(PEt_3)_6]^+$. Solid solutions of the two cluster cations have been isolated as the BPh_4^- salt. The deuteriated derivative $[Co_6(\mu_3\text{-}S)_7(\mu_3\text{-}D)(PEt_3)_6]^+$ has been prepared for comparison. The compounds have been characterized by ^1H, ^{31}P NMR, mass spectrometry and electrochemical measurements. The molecular structure of a sample of composition $[Co_6(\mu_3\text{-}S)_7(\mu_3\text{-}H)(PEt_3)_6]_{0.7}[Co_6(\mu_3\text{-}S)_8(PEt_3)_6]_{0.3}[BPh_4]$ has been determined by single-crystal X-ray diffraction. It consists of a solid solution of $[Co_6(\mu_3\text{-}S)_7(\mu_3\text{-}H)(PEt_3)_6]^+$ and $[Co_6(\mu_3\text{-}S)_8(PEt_3)_6]^+$. The cation $[Co_6(\mu_3\text{-}S)_7(\mu_3\text{-}H)(PEt_3)_6]_{0.7}[Co_6(\mu_3\text{-}S)_8(PEt_3)_6]_{0.3}^+$ is isostructural with the series $[M_6(\mu_3\text{-}S)_8(PEt_3)_6]^{n+}$, having a metal–metal separation averaging 2.739(8) Å. The electronic structure of the novel hydrido-derivative has been investigated through density functional calculations.

Metal–chalcogen clusters represent a fascinating topic of modern co-ordination chemistry.[1] Indeed these compounds are involved in fundamental biological processes (*e.g.* metal–sulfur clusters are contained in the active sites of several naturally occurring enzymes), constitute the structural units of solid materials showing peculiar physical properties (*e.g.* electrical conduction, ferromagnetism, *etc.*), and enter into heterogeneous catalytic processes (*e.g.* metal-catalysed hydrodesulfurization). On the other hand the elucidation of the synthetic, structural and theoretical aspects of their chemistry (*e.g.* synthesis mechanisms, electronic structures) still represents a challenge to inorganic chemists.

The family of clusters $[M_6(\mu_3\text{-}E)_8L_6]^{n+}$ [M = transition metal, E = chalcogenide, L = donor ligand (often PEt_3)] is continuously growing.[2] Particular interest in these clusters stems from the fact that they all contain an octahedral face-capped core M_6E_8, the shape of which is analogous to the building blocks of the Chevrel phases.[3] In these latter solids the Mo_6E_8 units are extensively interconnected to form extended structures. Since the axial terminal ligands L in $[M_6(\mu_3\text{-}S)_8L_6]^{n+}$ should prevent the formation of spatially extended structures, these systems are potentially good candidates for the investigation of the molecular and electronic structure of the 'isolated' $M_6(\mu_3\text{-}S)_8^{n+}$ moieties. In addition, it should be noted that these complexes behave as effective electron sponges, in that they usually exhibit multiple, non-destructive one-electron transfers.[2c,d,g–i,k]

A large number of octahedral clusters have been prepared by three different, independently developed, methods: (*i*) the reaction of H_2E with the iron(II) or cobalt(II) salts of poor co-ordinating anions, such as BF_4^-, ClO_4^-, in the presence of an excess of PEt_3; (*ii*) the reactions of $E(SiMe_3)_2$ with $[Co(PR_3)_2X_2]$ complexes; (*iii*) the reaction of $TePEt_3$ with low-valent transition-metal compounds in the presence of PEt_3. Unfortunately the mechanism of formation of these clusters is generally not clear, even when sometimes it is presumed to proceed through 'self-assembly' of the parent reagents. Only in the case of the molybdenum representative of this family, the synthesis has been really accomplished through the coupling of small metal–sulfur fragments.[2i]

We have been successful in the preparation of the novel cluster $[Co_6(\mu_3\text{-}S)_7(\mu_3\text{-}H)(PEt_3)_6]^+$ which can be isolated as the BPh_4^- salt, together with minor amounts of $[Co_6(\mu_3\text{-}S)_8(PEt_3)_6]^+$.[2d] As far as we know, only rare examples of octahedral clusters, in which the chalcogen atoms are partially substituted, namely $[Co_6(\mu\text{-}S)_6(\mu\text{-}I)_2(PEt_3)_6]^{2+}$[ref. 4(*a*)] or $[Re_6(\mu\text{-}S)_6(\mu\text{-}Cl)_2Cl_6]^{2-}$ [ref. 4(*b*)] have been previously reported. Moreover, although metal clusters containing bridging hydrides are numerous, no hydridometal–chalcogen clusters have been reported.

Experimental

General Considerations.—All reactions were performed under an atmosphere of dry nitrogen. Solvents were purified and dried by standard methods. The starting materials were reagent grade and used without further purification.

Synthesis of $[Co_6(\mu_3\text{-}S)_7(\mu_3\text{-}H)(PEt_3)_6]_x[Co_6(\mu_3\text{-}S)_8(PEt_3)_6]_{1-x}[BPh_4]$.—Triethylphosphine (1.3 cm^3, 8.8 mmol) was added to a deaerated solution of $Co(O_2CMe)_2\cdot 4H_2O$ (1 g,

* *Supplementary data available:* see Instructions for Authors, *J Chem. Soc., Dalton Trans.*, 1995, Issue 1, pp. xxv–xxx.

Non-SI unit employed: eV ≈ 1.60 × 10^{-19} J.

4 mmol) dissolved in a mixture of dimethylformamide (dmf) (15 cm^3) and EtOH (35 cm^3), and H_2S was bubbled through for 30 min at room temperature. After standing for 2 h a black powder separated. Sodium tetraphenylborate (700 mg, 2 mmol) was added to the decanted solution and after solvent evaporation under a current of nitrogen black crystals precipitated. These were recrystallized from CH_2Cl_2–EtOH (yield 550 mg) [Found: C, 43.9; H, 6.75; Co, 22.0; S, 14.6. Calc. for $C_{60}H_{110.7}BCo_6P_6S_{7.3}$ (sample used for X-ray analysis): C, 44.55; H, 6.9; Co, 21.9; S, 14.45%].

Synthesis of $[Co_6(\mu_3\text{-}S)_7(\mu_3\text{-}D)(PEt_3)_6]_x[Co_6(\mu_3\text{-}S)_8(PEt_3)_6]_{1-x}[BPh_4]$.—The compound was prepared as described above, using $Co(O_2CMe)_2{\cdot}4D_2O$, D_2S and deuteriated solvents (yield 55%) (Found: C, 44.0; H, 6.6; Co, 21.8. Calc. for $C_{60}H_{110}BCo_6D_{0.7}P_6S_{7.3}$: C, 44.5; H, 6.9; Co, 21.9%).

NMR Spectroscopy.—The ^1H and $^{31}P\text{-}\{^1H\}$ NMR spectra were recorded at 200.131 and 81.015 MHz respectively on a Bruker 200-AC spectrometer. Chemical shifts are relative to internal $SiMe_4$ (^1H) or external H_3PO_4 (^{31}P), with downfield values reported as positive. The $^1H\text{-}\{^{31}P\}$ NMR spectra were recorded on the same instrument equipped with a 5 mm inverse probe and a BFX-5 amplifier device.

Mass Spectrometry.—Mass spectrometry experiments were carried out on a two-sectors VG 70–250S instrument at acceleration voltage 8 kV, resolution 2000 $m/\Delta m$ (10% of valley). The instrument is equipped with a caesium-ion gun, as a source of primary ions, operating at anode potential 35 kV and current 2 μA. Collision-induced dissociation (CID) daughter-ion spectra were obtained by computer-controlled linked scans between the magnet and the electrostatic analysers. Argon was introduced in the collision cell located in the first field-free region until the intensity of the main beam was reduced to 50% of the original value. One drop of a solution obtained by dissolving a few micrograms of each complex in CH_2Cl_2 was placed on the stainless-steel tip of the probe, mixed with *m*-nitrobenzyl alcohol as a matrix, and exposed to the caesium-ion beam for the desorption.

Crystallography.—*Crystal data for* $[Co_6(\mu_3\text{-}S)_7(\mu_3\text{-}H)(PEt_3)_6]_{0.7}[Co_6(\mu_3\text{-}S)_8(PEt_3)_6]_{0.3}[BPh_4]$. $C_{60}H_{110.7}BCo_6P_6S_{7.3}$, $M = 1616.6$, triclinic, space group $P\bar{1}$, $a = 12.452(6)$, $b = 15.599(7)$, $c = 19.310(9)$ Å, $\alpha = 94.00(3)$, $\beta = 93.78(4)$, $\gamma = 92.42(4)°$, $U = 3729.3$ $Å^3$, $Z = 2$, $D_c = 1.440$ g cm^{-3}, μ(Mo-Kα) = 16.6 cm^{-1}, $\lambda = 0.7107$ Å. A black regular prism of dimensions 0.12 × 0.30 × 0.60 mm was mounted on an Enraf-Nonius CAD4 automatic diffractometer. The unit cell was determined by least-squares refinement of the setting angles of 25 reflections. Intensity data were collected by the ω–2θ scan method with scan speed ranging from 1.27 to 16.48° min^{-1} and scan width = 0.8 + 0.35 tan θ within $2\theta \leqslant 40°$. The standard deviations $\sigma(I)$ were calculated by using a value of 0.03 for the instability factor k,[5] and the data were corrected for Lorentz-polarization effects and for absorption.[6] 4137 Reflections, with $I > 3\sigma(I)$, were considered observed.

All the calculations were carried out on an HP 486 personal computer using SHELX 76[7] and ORTEP[8] programs. Atomic scattering factors for non-hydrogen and hydrogen atoms were taken from refs. 9 and 10 respectively. Corrections for anomalous dispersion effects, real and imaginary, were applied to the calculated structure-factor amplitudes.[11] Owing to the isomorphism with $[Co_6(\mu_3\text{-}S)_8(PEt_3)_6][BPh_4]$,[2d] the cobalt atom positions of the latter were used as starting parameters. Full-matrix least-squares refinements were carried out assigning anisotropic thermal parameters to cobalt, phosphorus and sulfur atoms and treating the phenyl rings as rigid groups. A Fourier-difference map showed that one out of the eight μ_3-bridging ligands has an electron density which is 25–30% that of the others. This fact, together with the results of mass and NMR spectroscopy, led to the hypothesis that these crystals are a solid solution of $[Co_6(\mu_3\text{-}S)_7(\mu_3\text{-}H)(PEt_3)_6]^+$ and $[Co_6(\mu_3\text{-}S)_8(PEt_3)_6]^+$, the only difference in the two cations being the presence in the μ_3-bridging position alternatively of an hydride and a sulfur ligand. The above-mentioned peak was attibuted to the sulfur ligand which was refined with a population parameter of 0.3. A peak 0.6 Å away from this sulfur and 1.6–2.0 Å from the three cobalt atoms was tentatively, but unsuccessfully refined as the hydride ligand. The function minimized was $\Sigma w(|F_o| - |F_c|)^2$, where $w = 1/\sigma^2(F_o)$. At convergence R and $R' = 0.051$ and 0.050 respectively. Final atomic parameters are given in Table 1.

Additional material available from the Cambridge Crystallographic Data Centre comprises thermal parameters and remaining bond lengths and angles.

Electrochemistry.—Materials and apparatus for electrochemistry have been described elsewhere.[12] Potentials are referred to the saturated calomel electrode (SCE). Under the present experimental conditions the ferrocene–ferrocenium couple is located at +0.45, +0.48 and +0.54 V in dichloromethane, 1,2-dimethoxyethane and tetrahydrofuran, respectively. Electrochemical measurements were performed on PF_6^- salts. Samples of $[Co_6(\mu_3\text{-}S)_7(\mu_3\text{-}H)(PEt_3)_6]_x[Co_6(\mu_3\text{-}S)_8(PEt_3)_6]_{1-x}[PF_6]{\cdot}EtOH$ were prepared by metathesis of the parent tetraphenylborate derivative with $TlPF_6$ in CH_2Cl_2–ethanol solution.

Density Functional Calculations.—Density functional calculations were performed using the ADF program developed by Baerends and co-workers,[13–15] in the local density approximation. The Volsko–Wilk–Nusair approximation[16] for the exchange correlation was used throughout. Non-local corrections to the correlation energy were applied in the form suggested by Stoll *et al.*[17] All the calculations were performed on the model complex $[Co_6(\mu_3\text{-}S)_7(\mu_3\text{-}H)(PH_3)_6]$, in which PH_3 has been substituted for PEt_3. This procedure has already been applied successfully to study the geometrical, electronic and magnetic structure of a series of related complexes $[Co_6(\mu_3\text{-}X)_8(PEt_3)_6]^{n+}$ (X = S, Se or Te; n = 0–2).[18]

The geometry of $[Co_6(\mu_3\text{-}S)_7(\mu_3\text{-}H)(PH_3)_6]$ was optimized using spin-restricted calculations. The following primitive Slater-type orbital (STO) basis functions have been used: 1s single ζ for H of the PH_3 groups; 1s double ζ for the μ_3-H; 3s and 3p double ζ for S and P; 4s and 3d triple ζ and 4p single ζ for Co. The core state was kept 'frozen' with the configurations $1s^22s^22p^6$ for S and P and $1s^22s^22p^63s^23p^6$ for Co. Exponents of the STOs and fit functions and coefficients for the Coulomb potential were taken from the default library contained in ADF. Energy gradients were minimized using the Broyden–Fletcher–Goldfarb–Shanno algorithm.[19] During the calculations the overall symmetry of the molecule was fixed at C_{3v}. The positions of the Co, S and μ_3-H atoms are referred, by distance and azimuthal angle (θ), to the centre of the molecular unit which is an inversion centre in the $[Co_6(\mu_3\text{-}X)_8(PH_3)_6]$ complexes. In this way the geometry of the $Co_6(\mu_3\text{-}S)_7(\mu_3\text{-}H)$ core is defined by six symmetry-independent distances and four azimuthal angles, the μ_3-H and the S atoms lying on the C_3 axis. The labelling of the atoms is shown in Fig. 1. In order to minimize the number of parameters, and to reduce the computer time, we kept the Co–P distances fixed at 2.14 Å and the S–Co–P angles at 101°. The geometry of the phosphine was frozen to a tetrahedron. The effect of these constraints on the geometrical optimization of the $[Co_6(\mu_3\text{-}X)_8(PH_3)_6]$ clusters has been considered in some detail[18] and found to have negligible consequences. In the previous work[18] the computed geometries are in nice agreement with the experimental ones, the largest deviations being in the Co–Co distances. The largest deviation from the experimental Co–Co distances was computed for X = Te as 4.6%, only 3.4% for X = S.

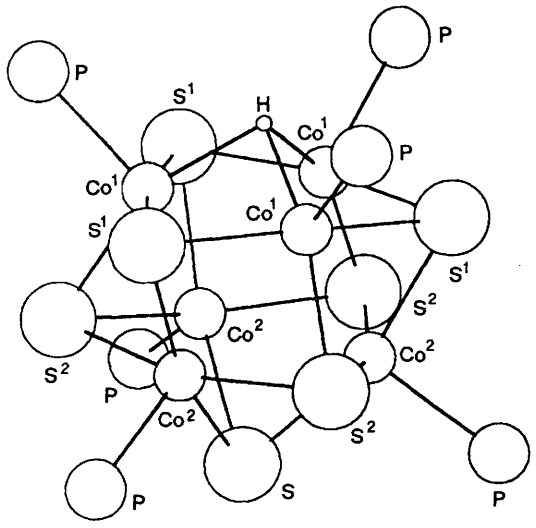

Fig. 1 Computed geometry for $[Co_6(\mu_3\text{-}S)_7(\mu_3\text{-}H)(PH_3)_6]^+$ with the labelling of the symmetry non-equivalent atoms

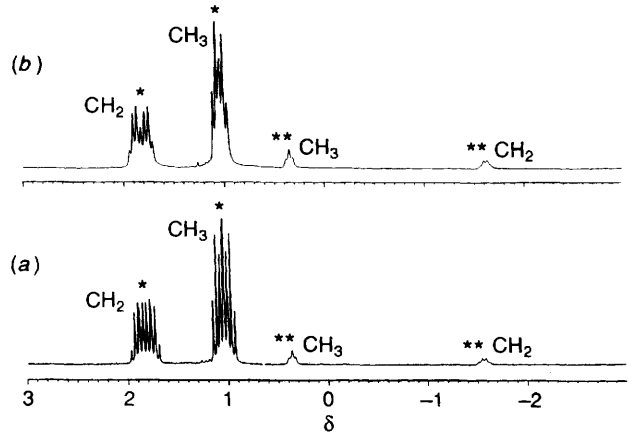

Fig. 2 Proton (*a*) and $^1H\text{-}\{^{31}P\}$ (*b*) NMR spectra (PEt_3 region, CD_2Cl_2, room temperature) of $[Co_6(\mu_3\text{-}S)_7(\mu_3\text{-}H)(PEt_3)_6]_{0.7}[Co_6(\mu_3\text{-}S)_8(PEt_3)_6]_{0.3}[BPh_4]$; * refers to $[Co_6(\mu_3\text{-}S)_7(\mu_3\text{-}H)(PEt_3)_6]^+$ and ** to $[Co_6(\mu_3\text{-}S)_8(PEt_3)_6]^+$

Results and Discussion

Synthesis.—The reaction of $Co(O_2CMe)_2\cdot 4H_2O$ with PEt_3 (molar ratio 1:3) and a large excess of H_2S, at room temperature, in dmf, affords a dark brown solution from which, after addition of $NaBPh_4$ and suitable work-up, black crystals can be separated. The material readily dissolves in polar organic solvents such as dichloromethane, acetone and acetonitrile, but it is fairly soluble also in hot benzene. The elemental analyses, which are practically analogous for samples from different preparations, slightly differ from those of $[Co_6S_8(PEt_3)_6][BPh_4]$,[2d] only the percentage of S being markedly smaller. A further treatment of the above material with H_2S in CH_2Cl_2 did not afford any significant change in its composition.

NMR Spectroscopy.—The ^1H NMR spectrum of this compound, apart from the resonances due to the BPh_4^- anion, shows two complicated, well resolved, multiplets centred at δ 1.85 and 1.05, two broad signals at δ 0.35 (t) and −1.61 (q, $^3J_{HH}$ = 8 Hz) [Fig. 2(*a*)] and a broad singlet at δ −31.7 (not shown). The two broad signals are due to the CH_2 and CH_3 protons of the known paramagnetic cluster $[Co_6(\mu_3\text{-}S)_8(PEt_3)_6]^+$.[2d,20] The other two low-field resonances, which have relative intensities in the ratio 2:3, can be attributed to the PEt_3 protons of a new diamagnetic species. Finally the very high-field signal is consistent with the presence of a hydridic hydrogen. This assignment has been fully confirmed by the ^1H NMR spectrum of the deuteriated derivative prepared by an analogous reaction, using D_2S, $Co(O_2CMe)_2\cdot 4D_2O$ and deuteriated solvents. The $^1H\text{-}\{^{31}P\}$ NMR spectrum shows a simplified pattern for the PEt_3 resonances of the diamagnetic species, consisting of a doublet of equally intense quartets ($^3J_{HH}$ = 7.5 Hz) centred at δ 1.85 and a doublet of equally intense triplets at δ 1.05 [Fig. 2(*b*)]. This result clearly indicates that the new species contains two equal-intensity sets of magnetically non-equivalent triethylphosphine ligands, and is in accord with the $^{31}P\text{-}\{^1H\}$ spectrum which shows two broad singlets (*ca.* 1:1) at δ 47.9 and 44.3. The ^1H NMR spectra of samples of this material from different preparations are substantially similar, also with respect to the ratio of the diamagnetic to the paramagnetic species. Unfortunately these spectra do not allow the determination of the exact composition of the mixture, because of the broad shape of the paramagnetic signals.*

The spectra show that the diamagnetic species slowly decomposes in solution, also under a nitrogen atmosphere.

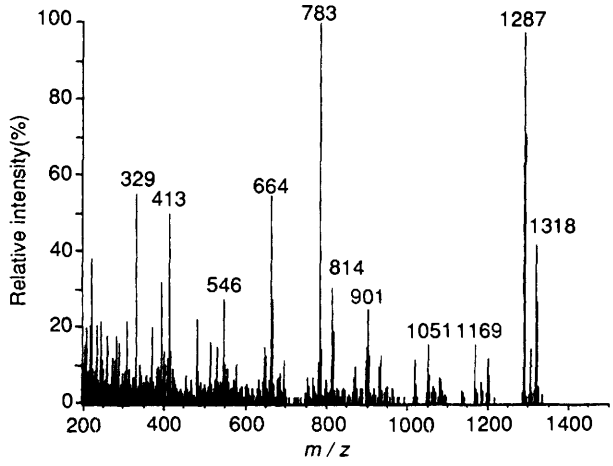

Fig. 3 Liquid secondary ion (LSI) mass spectrum obtained from the solid solution of $[Co_6(\mu_3\text{-}S)_7(\mu_3\text{-}H)(PEt_3)_6]_{0.7}[Co_6(\mu_3\text{-}S)_8(PEt_3)_6]_{0.3}[BPh_4]$

Mass Spectrometry.—The mass spectrum obtained by desorption of the solid solution of $[Co_6(\mu_3\text{-}S)_7(\mu_3\text{-}H)(PEt_3)_6]_{0.7}[Co_6(\mu_3\text{-}S)_8(PEt_3)_6]_{0.3}[BPh_4]$ (Fig. 3) shows an intense isotopic cluster centred at *m/z* 1287 and another less-intense one at *m/z* 1318. The highest-mass ion represents the molecular ion of the species $[Co_6(\mu_3\text{-}S)_8(PEt_3)_6]^+$ (calc. for $C_{36}H_{90}Co_6P_6S_8$ *m/z* 1318), while that at *m/z* 1287 is attributable to the molecular ion of the novel cluster $[Co_6(\mu_3\text{-}S)_7(\mu_3\text{-}H)(PEt_3)_6]^+$ (calc. for $C_{36}H_{91}Co_6P_6S_7$ *m/z* 1287). Their relative intensities are 45 and 97% respectively, in good agreement with the composition deduced from X-ray diffraction. The use of BPh_4 or PF_6 salts does not produce any change in the mass spectrum.

When the solid obtained by the same reaction by using deuteriated reagents and solvents is subjected to LSIMS desorption the peak at *m/z* 1318 is still present, while that at *m/z* 1287 is shifted to *m/z* 1288, in accordance with the presence of an hydride ligand. Series of fragment ions, corresponding to subsequent losses of 118 and 150 mass units, are present. Owing to the presence of isobaric species having 150 mass units, *i.e.* Co_2S and S + PEt_3, which might be reasonably involved in the fragmentation pathways, the correct assignment of each ion

* Integration of the signals of our ^1H NMR spectra of solutions containing known comparable amounts of $[Co_6S_8(PEt_3)_6]^+$ and a reference diamagnetic compound invariably indicates a wrong ratio for the reference compound to the cluster cation, the latter being remarkably underestimated (10–20%).

was deduced by study of the isostructural cluster $[Co_6(\mu_3\text{-}S)_8(PPh_3)_6]^+$.[2f] Its mass spectrum shows fragment ions differing by 262 and 294 mass units due to successive losses of PPh_3 and S + PPh_3 respectively. Fragmentations attributable to the elimination of Co_2S are not detectable.

Tandem mass spectrometry allowed us to study separately the fragmentations of each of the two species $[Co_6(\mu_3\text{-}S)_7(\mu_3\text{-}H)(PEt_3)_6]^+$ and $[Co_6(\mu_3\text{-}S)_8(PEt_3)_6]^+$ and has been used to determine the parent–daughter relationships among the various ions present in the mass spectrum of the solid solution. In particular, collision-induced dissociations of each molecular and fragment ion occurring in the first field-free region have been studied by linked scans between the two analysers (Fig. 4). Both the molecular ions of the species $[Co_6(\mu_3\text{-}S)_7(\mu_3\text{-}H)(PEt_3)_6]^+$ and $[Co_6(\mu_3\text{-}S)_8(PEt_3)_6]^+$ fragment by loss of one or two PEt_3 groups, yielding ions at *m/z* 1169, 1051 and 1200, 1082 respectively. The other ions present in their CID daughter-ion spectra are due to two or more successive reactions (Schemes 1 and 2).

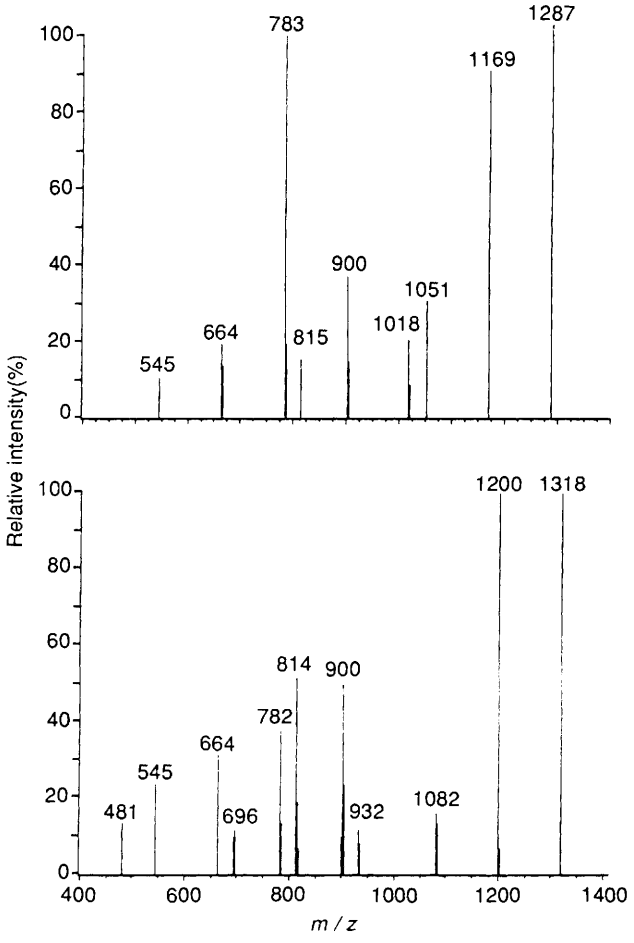

Fig. 4 The CID daughter-ion spectra of the molecular ions of the species $[Co_6(\mu_3\text{-}S)_7(\mu_3\text{-}H)(PEt_3)_6]^+$ (top) and $[Co_6(\mu_3\text{-}S)_8(PEt_3)_6]^+$ (bottom)

As regards $[Co_6(\mu_3\text{-}S)_8(PEt_3)_6]^+$, the first two generations of fragment ions lose PEt_3 or S + PEt_3 (Scheme 1). It is noteworthy that the CID daughter-ion spectra, obtained by selecting each fragment ion formed in the ion source as the main beam, do not show the loss of sulfur, but that of S + PEt_3. It is reasonable to suppose that the fragmentation pathway involves two successive reactions, that is the losses of sulfur and PEt_3, which occur sufficiently rapidly in comparison with the flight time of the ions in the first field-free region, thus allowing one to detect only their final product ions.

In the case of the species $[Co_6(\mu_3\text{-}S)_7(\mu_3\text{-}H)(PEt_3)_6]^+$ the loss of the hydride group occurs just after the loss of one or two PEt_3 groups from the molecular ion, producing the ions at *m/z* 1018 and 900 respectively. On the other hand, the ion at *m/z* 783, which constitutes the base peak in the mass spectrum of the solid solution, is formed by the ion at *m/z* 933 through the losses of S and PEt_3, and it retains the hydride ligand.

None of the fragmentation pathways involve the cobalt atoms, at least till all the PEt_3 groups have been lost. The fragmentation pathways of $[Co_6(\mu_3\text{-}S)_7(\mu_3\text{-}H)(PEt_3)_6]^+$ and $[Co_6(\mu_3\text{-}S)_8(PEt_3)_6]^+$ produce the clusters $[Co_6S_6]^+$ and $[Co_6S_4]^+$ at *m/z* 545 and 481 respectively.

The Crystal Structure.—Many crystals from different preparations were examined by X-ray diffraction and all were found to be identical and isomorphous with those of the paramagnetic cluster $[Co_6(\mu_3\text{-}S)_8(PEt_3)_6][BPh_4]$.[2d] The molecular structure determination of a representative sample showed (see Experimental section) that the novel diamagnetic species is $[Co_6(\mu_3\text{-}S)_7(\mu_3\text{-}H)(PEt_3)_6][BPh_4]$.

The molecular structure consists of a solid solution of the cations $[Co_6(\mu_3\text{-}S)_7(\mu_3\text{-}H)(PEt_3)_6]^+$ and $[Co_6(\mu_3\text{-}S)_8(PEt_3)_6]^+$ together with $[BPh_4]^-$ anions. Fig. 5 shows a perspective view of the cation and Tables 2 and 3 report selected bond distances and angles. The cation is isostructural with the members of the series $[M_6(\mu_3\text{-}S)_8(PEt_3)_6]^{n+}$ (M = Fe, *n* = 1

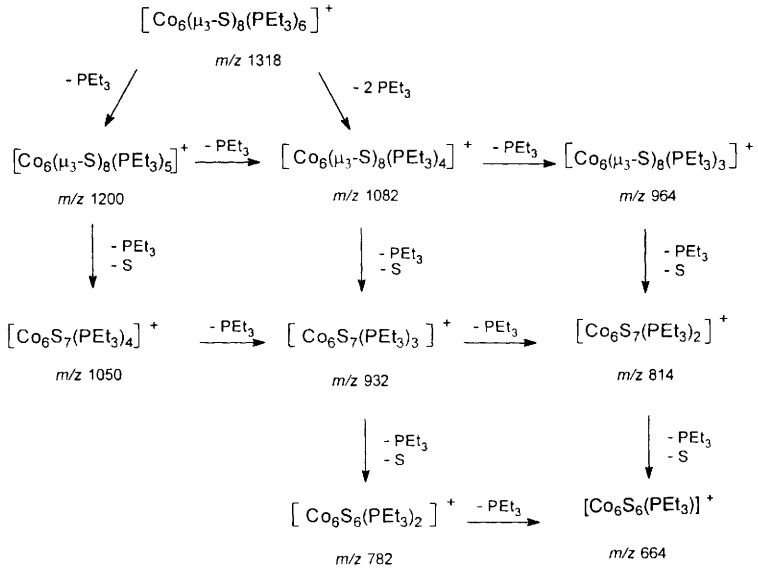

Scheme 1

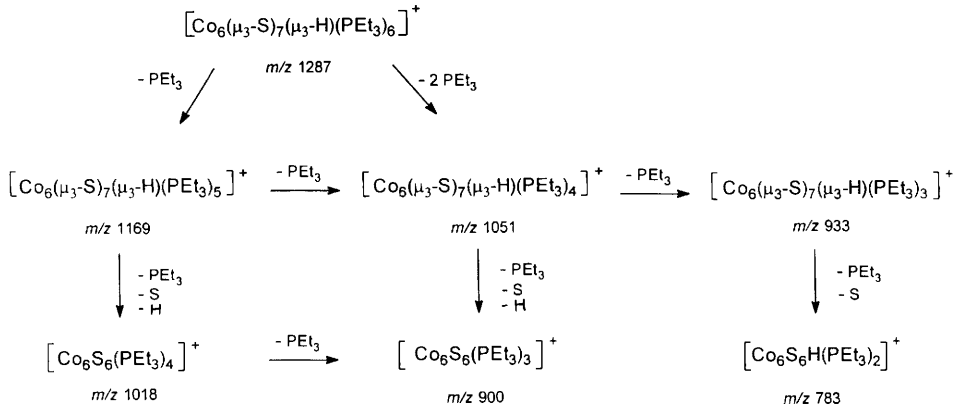

Scheme 2

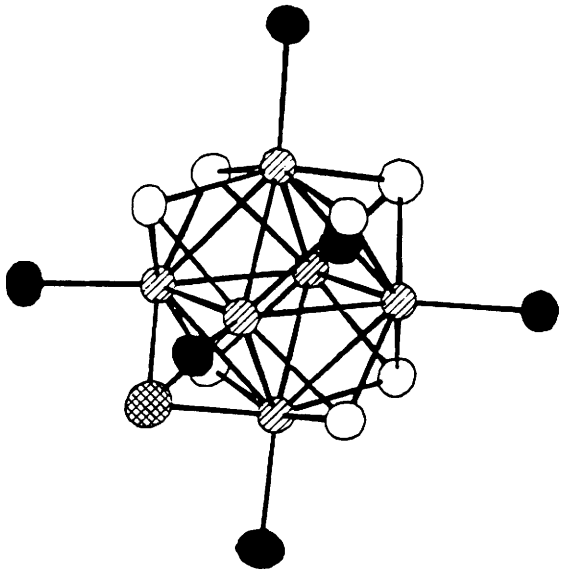

Fig. 5 Perspective view of the cluster cation $[Co_6(\mu_3\text{-}S)_7(\mu_3\text{-}H)(PEt_3)_6]_{0.7}[Co_6(\mu_3\text{-}S)_8(PEt_3)_6]_{0.3}^{+}$. Dashed, black and white circles represent cobalt, phosphorus and sulfur atoms respectively. The cross-hatched circle corresponds to the position of the sulfur atom, refined with population parameter of 0.3. The hydride ligand was not located

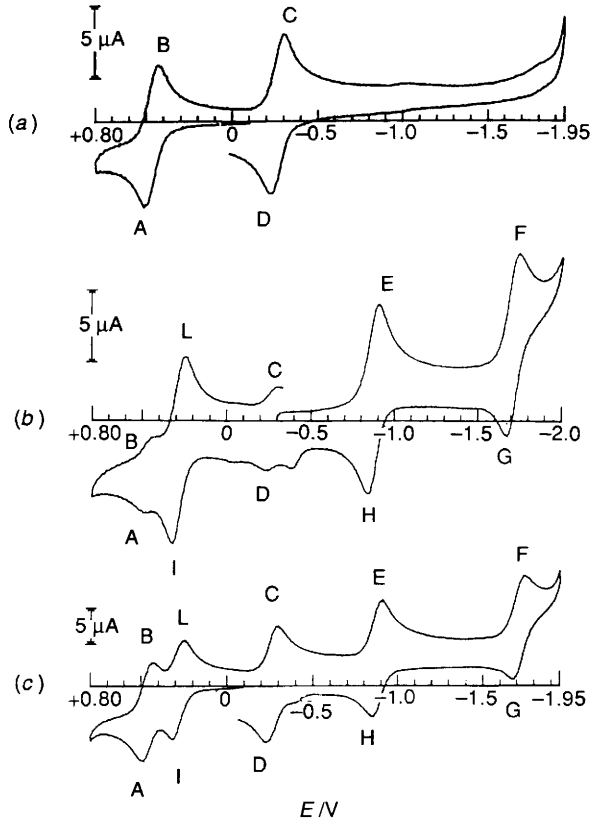

Fig. 6 Cyclic voltammetric responses recorded at a platinum electrode on thf solutions containing $[NBu_4][ClO_4]$ (0.2 mol dm^{-3}) and (*a*) $[Co_6(\mu_3\text{-}S)_8(PEt_3)_6][PF_6]$ (7.1×10^{-4} mol dm^{-3}); (*b*) $[Co_6(\mu_3\text{-}S)_7(\mu\text{-}H)(PEt_3)_6]_x[Co_6(\mu_3\text{-}S)_8(PEt_3)_6]_{1-x}[PF_6]$ (6.5×10^{-4} mol dm^{-3}); (*c*) $[Co_6(\mu_3\text{-}S)_7(\mu_3\text{-}H)(PEt_3)_6]_x[Co_6(\mu_3\text{-}S)_8(PEt_3)_6]_{1-x}[PF_6]$ (6.5×10^{-4} mol dm^{-3}) and $[Co_6(\mu_3\text{-}S)_8(PEt_3)_6][PF_6]$ (6.7×10^{-4} mol dm^{-3}). Scan rate 0.2 V s^{-1}

or 2; M = Co, $n = 0$ or 1)[2a,d] the only difference being the presence in one μ_3-bridging site alternatively of one hydride or one sulfur ligand in a ratio of *ca.* 7:3 according to the results of the least-squares refinement. This partial substitution leaves the octahedral framework substantially unchanged, which maintains approximate O_h symmetry, the Co–Co–Co angles deviating only slightly from the idealized values of 60 and 90°. The metal–metal separations, averaging 2.739(8) Å, are significantly shorter than those reported for the parent clusters $[Co_6(\mu_3\text{-}S)_8(PEt_3)_6]^{n+}$ [$n = 1$, 2.794(3); $n = 0$, 2.817(3) Å].[2d] The depopulation of antibonding molecular orbitals, which occurs on substituting one sulfur with one hydride ligand, may account for the above shortening.

These results are in full agreement with those obtained for the cluster $[Co_6(\mu_3\text{-}S)_6(\mu_3\text{-}I)_2(PEt_3)_6]^{2+}$, where the substitution of two bridging sulfurs by two iodine ligands scarcely affects the structural parameters.[4a]

Several cluster compounds containing an hydride ligand μ_3 bridging a triangle of metal atoms have been reported.[21] These are generally carbonyl clusters, but as far as we know this is the first example of an hydridometal–sulfur cluster.

Electrochemistry.—Figs. 6 and 7 compare the electrochemical response of $[Co_6S_7(H)(PEt_3)_6]^{+}$ with that of the precursor $[Co_6S_8(PEt_3)_6]^{+}$, either in tetrahydrofuran or in dichloromethane solutions. Tetrahydrofuran (thf) proved to be useful to gain information on the most cathodic response exhibited by $[Co_6S_7(H)(PEt_3)_6]^{+}$, whereas dichloromethane provided the best defined anodic responses.

With reference to the responses of the original solid solution of $[Co_6S_7(H)(PEt_3)_6]^{+}$ shown in Figs. 6(*b*) and 7(*b*), it is evident that, in accordance with the above discussed spectroscopic evidence, the minor peak systems A/B, C/D, M/N, which accompany the major responses E/H, F/G, I/L and O/P, are attributable to the presence of minor amounts of $[Co_6S_8(PEt_3)_6]^{+}$. This is supported by the voltammetric profiles shown in Figs. 6(*c*) and 7(*c*) recorded after addition of the known $[Co_6S_8(PEt_3)_6]^{+}$.

Table 1 Final positional parameters ($\times 10^4$) for $[Co_6(\mu_3\text{-}S)_7(\mu_3\text{-}H)(PEt_3)_6]_{0.7}[Co_6(\mu_3\text{-}S)_8(PEt_3)_6]_{0.3}[BPh_4]$

Atom	x	y	z	Atom	x	y	z
Co(1)	2 038(1)	2 443(1)	2 450(1)	C(22)	3 670(15)	6 263(12)	2 153(11)
Co(2)	2 874(1)	1 042(1)	3 008(1)	C(23)	4 690(14)	5 362(11)	3 597(10)
Co(3)	3 985(1)	1 876(1)	2 071(1)	C(24)	3 719(16)	5 445(12)	4 061(11)
Co(4)	3 888(1)	3 390(1)	2 850(1)	C(25)	1 390(12)	2 001(10)	5 185(8)
Co(5)	2 768(1)	2 538(1)	3 820(1)	C(26)	985(15)	2 222(12)	5 920(10)
Co(6)	4 750(1)	1 975(1)	3 420(1)	C(27)	3 214(11)	3 221(9)	5 531(8)
P(1)	519(3)	2 620(3)	1 859(2)	C(28)	4 022(13)	2 513(10)	5 708(9)
P(2)	2 299(3)	−287(2)	3 008(2)	C(29)	1 314(12)	3 809(9)	4 899(8)
P(3)	4 501(3)	1 529(3)	1 044(2)	C(30)	185(13)	3 632(11)	4 489(9)
P(4)	4 383(3)	4 725(2)	2 766(2)	C(31)	7 347(11)	1 419(9)	3 365(8)
P(5)	2 180(3)	2 879(2)	4 836(2)	C(32)	8 452(12)	1 223(10)	3 748(9)
P(6)	6 309(3)	1 783(2)	3 949(2)	C(33)	6 304(10)	1 014(9)	4 619(8)
S(1)	3 189(3)	3 045(2)	1 771(2)	C(34)	6 034(11)	55(9)	4 313(8)
S(2)	2 224(3)	3 594(2)	3 180(2)	C(35)	6 957(11)	2 718(9)	4 472(8)
S(3)	1 396(3)	1 720(2)	3 287(2)	C(36)	7 254(13)	3 491(10)	4 022(9)
S(4)	4 535(3)	811(2)	2 684(2)	B	8 715(13)	6 925(11)	1 566(10)
S(5)	5 354(3)	2 703(2)	2 565(2)	C(1,1)	7 851(6)	7 612(7)	1 922(6)
S(6)	4 391(3)	3 237(3)	3 965(2)	C(2,1)	8 279(6)	8 371(7)	2 280(6)
S(7)	3 576(3)	1 346(2)	4 076(2)	C(3,1)	7 598(6)	8 946(7)	2 593(6)
S(8)*	2349(7)	1 175(6)	1 911(5)	C(4,1)	6 488(6)	8 762(7)	2 549(6)
C(1)	−529(12)	3 032(10)	2 407(8)	C(5,1)	6 060(6)	8 004(7)	2 191(6)
C(2)	−1 635(14)	3 200(11)	2 009(10)	C(6,1)	6 741(6)	7 429(7)	1 878(6)
C(3)	−84(15)	1 629(12)	1 371(10)	C(1,2)	9 631(8)	7 459(5)	1 115(6)
C(4)	−413(16)	898(13)	1 826(11)	C(2,2)	10 553(8)	7 035(5)	944(6)
C(5)	578(15)	3 335(12)	1 131(11)	C(3,2)	11 321(8)	7 440(5)	568(6)
C(6)	900(17)	4 244(14)	1 393(12)	C(4,2)	11 169(8)	8 269(5)	363(6)
C(7)	3 235(11)	−925(9)	3 505(8)	C(5,2)	10 248(8)	8 693(5)	534(6)
C(8)	2 840(12)	−1 890(10)	3 559(9)	C(6,2)	9 479(8)	8 288(5)	910(6)
C(9)	956(11)	−479(9)	3 361(8)	C(1,3)	9 294(6)	6 452(6)	2 232(5)
C(10)	981(12)	−204(10)	4 146(9)	C(2,3)	8 673(6)	5 831(6)	2 533(5)
C(11)	2 071(12)	−881(9)	2 152(8)	C(3,3)	9 102(6)	5 430(6)	3 106(5)
C(12)	3 150(12)	−1 093(10)	1 805(9)	C(4,3)	10 151(6)	5 649(6)	3 377(5)
C(13)	5 366(14)	593(11)	954(10)	C(5,3)	10 771(6)	6 270(6)	3 077(5)
C(14)	6 501(15)	796(12)	1 333(11)	C(6,3)	10 343(6)	6 672(6)	2 504(5)
C(15)	5 202(14)	2 441(11)	667(10)	C(1,4)	8 107(7)	6 196(7)	966(5)
C(16)	5 572(17)	2 229(14)	−96(12)	C(2,4)	8 476(7)	5 363(7)	913(5)
C(17)	3 332(16)	1 312(13)	355(11)	C(3,4)	8 020(7)	4 763(7)	397(5)
C(18)	2 693(20)	553(16)	466(14)	C(4,4)	7 194(7)	4 994(7)	−67(5)
C(19)	5 680(12)	4 932(10)	2 378(9)	C(5,4)	6 824(7)	5 827(7)	−14(5)
C(20)	5 651(14)	4 650(12)	1 588(10)	C(6,4)	7 281(7)	6 427(7)	502(5)
C(21)	3 375(13)	5 301(10)	2 252(9)				

* Population parameter 0.3.

$$[Co_6S_7(H)(PEt_3)_6]^{3+} \underset{-e}{\overset{+e}{\rightleftharpoons}} [Co_6S_7(H)(PEt_3)_6]^{2+} \underset{-e}{\overset{+e}{\rightleftharpoons}}$$

$$[Co_6S_7(H)(PEt_3)_6]^{+} \underset{-e}{\overset{+e}{\rightleftharpoons}} [Co_6S_7(H)(PEt_3)_6] \underset{-e}{\overset{+e}{\rightleftharpoons}}$$

$$[Co_6S_7(H)(PEt_3)_6]^{-}$$

Scheme 3

Controlled-potential coulometric tests demonstrated that the electron transfers corresponding to the peak systems E/H and I/L involve one electron per molecule and are chemically reversible. In contrast, in the time window of macroelectrolysis, the most anodic as well as the most cathodic redox changes (namely, O/P and F/G, respectively) lead to decomposition of the molecule, probably also because of the proximity of the solvent discharge.

In summary, at least in the short times of cyclic voltammetry, $[Co_6S_7(H)(PEt_3)_6]^+$ undergoes the electron-transfer sequence in Scheme 3, which is by far the most extended one within the class of either $M_6E_8L_6$ species[2c,d,g-i,k] or the sulfur-substituted derivatives $M_6E_{8-n}L_{6+n}$.[4b]

Since in tetrahydrofuran solution some electrode poisoning occurred after a few cyclic voltammetric scans, a detailed analysis of the diagnostic parameters governing the most stable electrochemical redox changes {*i.e.*, $[Co_6S_7(H)(PEt_3)_6]^{2+/+/0}$} was performed in dichloromethane solution. In these redox changes the peak current ratio $i_{p\,(backward)}:i_{p\,(forward)} = 1:1$, independent of the scan rate (which varied from 0.02 to 10.24 V s^{-1}). Correspondingly, the peak-to-peak separation was around 70 mV up to 0.5 V s^{-1}, then progressively increased to 170 and to 126 mV for the $[Co_6S_7(H)(PEt_3)_6]^{+/2+}$ and $[Co_6S_7(H)(PEt_3)_6]^{+/0}$ processes, respectively, likely because of uncompensated solution resistances. In both cases the current function $i_{p\,(forward)}/v^{\frac{1}{2}}$ remained substantially constant. These data are consistent with one-electron transfers which very closely approach electrochemical reversibility.[22] As a consequence, it does not seem unreasonable to hypothesize[23] that the one-electron removal as well as the one-electron addition do not cause important structural changes with respect to the above-discussed geometry of $[Co_6S_7(H)(PEt_3)_6]^+$, as we verified for the $[Fe_6S_8(PEt_3)_6]^{2+/+}$ [ref. 2(*c*)] and $[Co_6S_8(PEt_3)_6]^{+/0}$ [ref. 2(*d*)] redox partners.

Table 4 summarizes the redox potentials of the above electron transfers in different non-aqueous solutions, also with respect to those of the precursor $[Co_6S_8(PEt_3)_6]^+$. It is clear that, under the same electrostatic conditions, the simple substitution of one sulfur for one hydride atom deeply affects the redox properties, not only causing significant shifts in the electrode potentials of corresponding electron transfers, but also enabling access to one more, relatively stable, redox congener.

Chemical Oxidation.—The two clusters can easily be oxidized by iodine in dichloromethane solution. In the ^1H NMR spectrum of a solution of a sample of the solid containing an excess of iodine (Fig. 8) the PEt_3 protons appear as broad signals shifted to high field characteristic of paramagnetic species: the couple of equal-intensity triplets at δ 0.63 and 0.23 and the corresponding two quartets at δ −0.82 and −2.86 can be attributed to the two sets of CH_3 and the two sets of CH_2P protons of $[Co_6(\mu_3\text{-}S)_7(\mu_3\text{-}H)(PEt_3)_6]^{2+}$ respectively, whereas the less-intense triplet and quartet at δ −0.45 and −5.9 are likely due to the CH_3 and CH_2P groups of $[Co_6(\mu_3\text{-}S)_8(PEt_3)_6]^{2+}$. The shifts of the above signals with respect to those of the corresponding singly charged species qualitatively indicate that the cation $[Co_6(\mu_3\text{-}S)_8(PEt_3)_6]^{2+}$ has a higher μ_{eff} than that of $[Co_6(\mu_3\text{-}S)_7(\mu_3\text{-}H)(PEt_3)_6]^{2+}$. Investigations of the isolation and characterization of these oxidized clusters are in progress.

Electronic Structure of $[Co_6(\mu_3\text{-}S)_7(\mu_3\text{-}H)(PH_3)_6]^+$.—The geometry computed for $[Co_6(\mu_3\text{-}S)_7(\mu_3\text{-}H)(PH_3)_6]^+$ is shown in Fig. 1 and computed bond distances and angles are collected in Table 5. The computed Co^1–H bond distance is well in the range observed for cobalt hydrides. The bond distances involving Co^1 are significantly smaller than those of Co^2 which are well in the range of distances observed in the $[Co_6(\mu_3\text{-}S)_8(PEt_3)_6]^{1+,0}$ complexes[2d] and compare well with those computed for $[Co_6(\mu_3\text{-}S)_8(PH_3)_6]^{n+}$ model compounds.

The substitution of a sulfide ion for an hydride one in the $Co_6(\mu_3\text{-}S)_8$ core does not produce severe alterations in the overall molecular structure, causing a rather small contraction in the bond distances around the metals bound to H. These results show that $Co_6(\mu_3\text{-}S)_8$ is a rather stable unit which can undergo even substitution of one of the chalcogen atoms without severe structural modifications.

The computed one-electron energy-level structure is shown in Fig. 9 in the form of density of states.[24] The curves are computed by artificially broadening each energy level with a Gaussian function of constant half-width 0.2. The overall appearance of the figure is similar to that computed for $[Co_6(\mu_3\text{-}S)_8(PH_3)_6]$. The lowest peak corresponds to P–H bonding orbitals. Between −11.7 and −9.3 eV a series of bonding Co–S–P orbitals is found. After a gap of ≈0.50 eV a band split by ≈2.2 eV is formed with contributions from the

Table 2 Selected distances (Å)

Co(1)–Co(2)	2.719(3)	Co(2)–Co(6)	2.741(2)
Co(1)–Co(3)	2.742(3)	Co(3)–Co(4)	2.721(3)
Co(1)–Co(4)	2.721(2)	Co(3)–Co(6)	2.706(3)
Co(1)–Co(5)	2.732(3)	Co(4)–Co(5)	2.784(3)
Co(2)–Co(3)	2.719(3)	Co(4)–Co(6)	2.760(3)
Co(2)–Co(5)	2.732(2)	Co(5)–Co(6)	2.792(2)
mean	2.739(8)*		
Co(1)–S(1)	2.226(4)	Co(4)–S(1)	2.224(4)
Co(1)–S(2)	2.199(4)	Co(4)–S(2)	2.236(4)
Co(1)–S(3)	2.208(4)	Co(4)–S(5)	2.236(4)
Co(1)–S(8)	2.230(9)	Co(4)–S(6)	2.234(5)
Co(2)–S(3)	2.238(4)	Co(5)–S(2)	2.228(4)
Co(2)–S(4)	2.237(4)	Co(5)–S(3)	2.237(4)
Co(2)–S(7)	2.198(4)	Co(5)–S(6)	2.246(4)
Co(2)–S(8)	2.201(9)	Co(5)–S(7)	2.222(4)
Co(3)–S(1)	2.206(4)	Co(6)–S(4)	2.222(4)
Co(3)–S(4)	2.213(4)	Co(6)–S(5)	2.221(4)
Co(3)–S(5)	2.215(4)	Co(6)–S(6)	2.241(4)
Co(3)–S(8)	2.264(9)	Co(6)–S(7)	2.236(4)
mean	2.226(3)		
Co(1)–P(1)	2.181(4)	Co(4)–P(4)	2.167(4)
Co(2)–P(2)	2.165(4)	Co(5)–P(5)	2.180(5)
Co(3)–P(3)	2.165(4)	Co(6)–P(6)	2.176(4)
mean	2.172(3)		

* The estimated errors on the means were calculated according to the formula $[\Sigma_n(d_n - d)^2/n(n-1)]^{\frac{1}{2}}$.

Table 3 Selected angles (°)

Co(2)–Co(1)–Co(3)	59.71(7)	Co(1)–Co(4)–Co(3)	60.52(6)	Co(1)–Co(3)–Co(2)	59.72(7)	Co(2)–Co(6)–Co(3)	59.87(7)
Co(2)–Co(1)–Co(4)	90.48(7)	Co(1)–Co(4)–Co(5)	59.49(7)	Co(1)–Co(3)–Co(4)	59.72(7)	Co(2)–Co(6)–Co(4)	89.18(7)
Co(2)–Co(1)–Co(5)	60.16(7)	Co(1)–Co(4)–Co(6)	89.96(7)	Co(1)–Co(3)–Co(6)	90.63(8)	Co(2)–Co(6)–Co(5)	59.17(6)
Co(3)–Co(1)–Co(4)	59.75(6)	Co(3)–Co(4)–Co(5)	89.74(7)	Co(2)–Co(3)–Co(4)	90.47(8)	Co(3)–Co(6)–Co(4)	59.70(7)
Co(3)–Co(1)–Co(5)	90.41(7)	Co(3)–Co(4)–Co(6)	59.17(7)	Co(2)–Co(3)–Co(6)	60.71(7)	Co(3)–Co(6)–Co(5)	89.89(7)
Co(4)–Co(1)–Co(5)	61.42(7)	Co(5)–Co(4)–Co(6)	60.47(7)	Co(4)–Co(3)–Co(6)	61.13(7)	Co(4)–Co(6)–Co(5)	60.20(6)
S(1)–Co(1)–S(2)	89.9(2)	S(1)–Co(4)–S(2)	89.0(1)	S(1)–Co(3)–S(4)	161.5(2)	S(4)–Co(6)–S(5)	88.8(2)
S(1)–Co(1)–S(3)	161.2(2)	S(1)–Co(4)–S(5)	88.0(1)	S(1)–Co(3)–S(5)	89.0(2)	S(4)–Co(6)–S(6)	159.2(2)
S(1)–Co(1)–S(8)	87.9(3)	S(1)–Co(4)–S(6)	159.0(2)	S(1)–Co(3)–S(8)	87.5(3)	S(4)–Co(6)–S(7)	87.7(1)
S(2)–Co(1)–S(3)	88.8(2)	S(2)–Co(4)–S(5)	159.5(2)	S(4)–Co(3)–S(5)	89.2(1)	S(5)–Co(6)–S(6)	88.1(2)
S(2)–Co(1)–S(8)	160.9(3)	S(2)–Co(4)–S(6)	87.7(2)	S(4)–Co(3)–S(8)	88.0(3)	S(5)–Co(6)–S(7)	159.1(2)
S(3)–Co(1)–S(8)	87.3(3)	S(5)–Co(4)–S(6)	87.9(2)	S(5)–Co(3)–S(8)	160.4(3)	S(6)–Co(6)–S(7)	87.8(2)
P(1)–Co(1)–S(1)	100.2(2)	P(4)–Co(4)–S(1)	100.3(2)	P(3)–Co(3)–S(1)	95.1(2)	P(6)–Co(6)–S(4)	101.7(1)
P(1)–Co(1)–S(2)	103.3(2)	P(4)–Co(4)–S(2)	98.1(2)	P(3)–Co(3)–S(4)	103.2(2)	P(6)–Co(6)–S(5)	97.2(1)
P(1)–Co(1)–S(3)	98.4(2)	P(4)–Co(4)–S(5)	102.4(2)	P(3)–Co(3)–S(5)	103.2(2)	P(6)–Co(6)–S(6)	99.1(2)
P(1)–Co(1)–S(8)	95.8(3)	P(4)–Co(4)–S(6)	100.8(2)	P(3)–Co(3)–S(8)	96.3(3)	P(6)–Co(6)–S(7)	103.7(2)
Co(1)–Co(2)–Co(3)	60.57(7)	Co(1)–Co(5)–Co(2)	59.69(7)	Co(1)–S(1)–Co(3)	76.5(1)	Co(3)–S(5)–Co(4)	75.4(1)
Co(1)–Co(2)–Co(5)	60.15(7)	Co(1)–Co(5)–Co(4)	59.09(7)	Co(1)–S(1)–Co(4)	75.4(1)	Co(3)–S(5)–Co(6)	75.2(1)
Co(1)–Co(2)–Co(6)	90.38(7)	Co(1)–Co(5)–Co(6)	89.07(8)	Co(3)–S(1)–Co(4)	75.8(1)	Co(4)–S(5)–Co(6)	76.5(1)
Co(3)–Co(2)–Co(5)	90.91(8)	Co(2)–Co(5)–Co(4)	88.87(8)	Co(1)–S(2)–Co(4)	75.7(1)	Co(4)–S(6)–Co(5)	76.8(1)
Co(3)–Co(2)–Co(6)	59.43(7)	Co(2)–Co(5)–Co(6)	59.50(6)	Co(1)–S(2)–Co(5)	76.2(1)	Co(4)–S(6)–Co(6)	76.2(1)
Co(5)–Co(2)–Co(6)	61.34(6)	Co(4)–Co(5)–Co(6)	59.33(6)	Co(4)–S(2)–Co(5)	77.2(1)	Co(5)–S(6)–Co(6)	76.9(1)
S(3)–Co(2)–S(4)	161.0(1)	S(2)–Co(5)–S(3)	87.4(1)	Co(1)–S(3)–Co(2)	75.4(1)	Co(2)–S(7)–Co(5)	76.3(1)
S(3)–Co(2)–S(7)	89.4(1)	S(2)–Co(5)–S(6)	87.6(1)	Co(1)–S(3)–Co(5)	75.8(1)	Co(2)–S(7)–Co(6)	76.4(1)
S(3)–Co(2)–S(8)	87.2(3)	S(2)–Co(5)–S(7)	158.0(2)	Co(2)–S(3)–Co(5)	75.2(1)	Co(5)–S(7)–Co(6)	77.5(1)
S(4)–Co(2)–S(7)	88.3(1)	S(3)–Co(5)–S(6)	158.4(2)	Co(2)–S(4)–Co(3)	75.3(1)	Co(1)–S(8)–Co(2)	75.7(3)
S(4)–Co(2)–S(8)	89.0(3)	S(3)–Co(5)–S(7)	88.8(1)	Co(2)–S(4)–Co(6)	75.9(1)	Co(1)–S(8)–Co(3)	75.2(3)
S(7)–Co(2)–S(8)	161.3(3)	S(6)–Co(5)–S(7)	88.0(1)	Co(3)–S(4)–Co(6)	75.2(1)	Co(2)–S(8)–Co(3)	75.0(3)
P(2)–Co(2)–S(3)	100.7(1)	P(5)–Co(5)–S(2)	103.6(2)				
P(2)–Co(2)–S(4)	98.1(1)	P(5)–Co(5)–S(3)	102.6(2)				
P(2)–Co(2)–S(7)	103.6(2)	P(5)–Co(5)–S(6)	99.1(2)				
P(2)–Co(2)–S(8)	95.1(3)	P(5)–Co(5)–S(7)	98.4(2)				

Table 4 Formal electrode potentials (in V *vs.* SCE) for the electron-transfer processes exhibited by the two monocations $[Co_6S_7(H)(PEt_3)_6]^+$ and $[Co_6S_8(PEt_3)_6]^+$ in different solvents. Values in parentheses indicate peak potentials for irreversible processes

	$E^{o\prime}$				
Complex	3+/2+	2+/+	+/0	0/−	Solvent
$[Co_6S_7(H)(PEt_3)_6]^{n+}$	(+0.95)	+0.28	−0.87	−1.70	thf
	+0.96	+0.10	−1.18	(−1.95)	CH_2Cl_2
	—	+0.28	−0.88	−1.71	dme *
$[Co_6S_8(PEt_3)_6]^{n+}$	(+1.02)	+0.47	−0.26		thf
	+1.06	+0.30	−0.54		CH_2Cl_2
	(+0.95)	+0.47	−0.27		dme

* 1,2-Dimethoxyethane.

Table 5 Selected bond distances (Å) and angles (°) computed for $[Co_6(\mu_3\text{-}S)_7(\mu_3\text{-}H)(PH_3)_6]^+$

Co^1–H	1.79	Co^2–S	2.25
Co^1–S^1	2.21	Co^2–S^2	2.23
Co^1–S^2	2.19	Co^2–S^1	2.24
Co^1–Co^1	2.56	Co^2–Co^2	2.73
Co^1–Co^2	2.61	$S^1 \cdots S^2$	3.13
H–S	2.77	$S \cdots S^2$	3.12
Co^1–H–Co^1	91	Co^2–S–Co^2	75

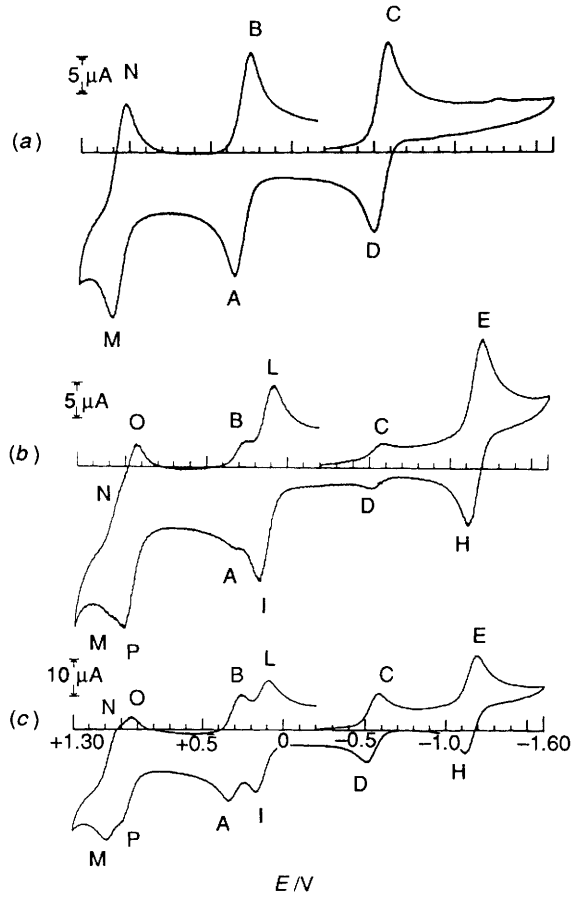

Fig. 7 Cyclic voltammetric responses recorded at a platinum electrode on CH_2Cl_2 solutions containing $[NBu_4][ClO_4]$ (0.2 mol dm^{-3}) and (*a*) $[Co_6(\mu_3\text{-}S)_8(PEt_3)_6][PF_6]$ (6.7×10^{-4} mol dm^{-3}); (*b*) $[Co_6(\mu_3\text{-}S)_7(\mu_3\text{-}H)(PEt_3)_6]_x[Co_6(\mu_3\text{-}S)_8(PEt_3)_6]_{1-x}[PF_6]$ (7.3×10^{-4} mol dm^{-3}); (*c*) $[Co_6(\mu_3\text{-}S)_7(\mu_3\text{-}H)(PEt_3)_6]_x[Co_6(\mu_3\text{-}S)_8(PEt_3)_6]_{1-x}[PF_6]$ (7.3×10^{-4} mol dm^{-3}) and $[Co_6(\mu_3\text{-}S)_8(PEt_3)_6][PF_6]$ (3.7×10^{-4} mol dm^3). Scan rate 0.2 V s^{-1}

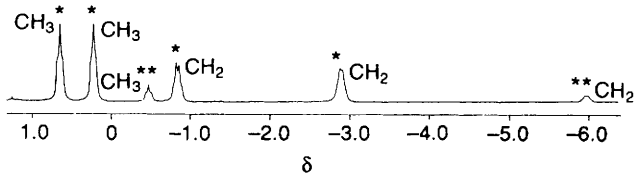

Fig. 8 Proton NMR spectrum (PEt_3 region, CD_2Cl_2, room temperature) of $[Co_6(\mu_3\text{-}S)_7(\mu_3\text{-}H)(PEt_3)_6]_{0.7}[Co_6(\mu_3\text{-}S)_8(PEt_3)]_{0.3}$-$[BPh_4]$ in the presence of an excess of iodine; * refers to $[Co_6(\mu_3\text{-}S)_7$-$(\mu_3\text{-}H)(PEt_3)_6]^{2+}$ and ** to $[Co_6(\mu_3\text{-}S)_8(PEt_3)_6]^{2+}$

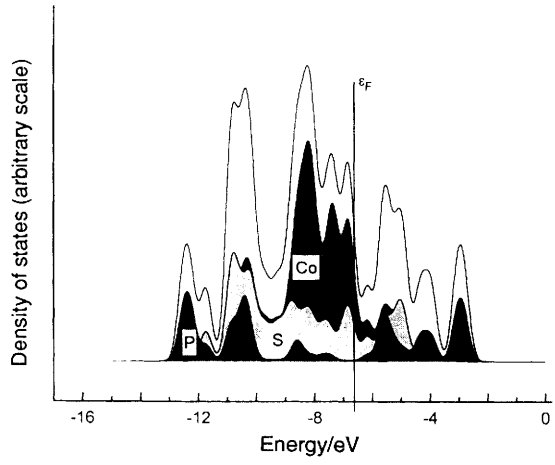

Fig. 9 Computed one-electron energy-level structure in the form of the density of states (see text). Partial values are shown to illustrate the separate contributions of the cobalt, phosphorus and sulfur atoms to the overlap population

3d orbitals of the cobalt atoms, the highest occupied orbitals, which form the Fermi level, ε_F, being weakly antibonding Co-S molecular orbitals. A series of antibonding Co-S and Co-P orbitals follows after a gap of $\approx$0.54 eV. The magnetic properties of the isostructural $[Co_6(\mu_3\text{-}X)_8(PEt_3)_6]^{n+}$ (X = S, Se or Te; n = 0–2)[18] and $[Fe_6(\mu_3\text{-}S)_8(PEt_3)_6]^{+,2+}$ complexes[24,25] have been successfully interpreted by determining the maximum possible multiplicity of the ground state by filling the one-electron energy levels up to the gap. This procedure suggests that the present compound has an $S = 0$ ground state. Excited states with spin multiplicity up to $S = 4$ are possible by filling the lowest unoccupied molecular orbital levels, but they are expected to be depopulated at room temperature and the $[Co_6(\mu_3\text{-}S)_7(H)(PEt_3)_6]^+$ complex is therefore expected to be diamagnetic, in agreement with the NMR results.

Density functional theory nicely accounts for geometrical variations in transition-metal clusters[18,26] and has been shown to be a helpful tool in understanding their magnetic properties.[24,25]

Acknowledgements

We are grateful to Mr. P. Innocenti and Mr. F. Nuzzi for technical assistance.

References

1 J. Dance and K. Fisher, *Prog. Inorg. Chem.*, 1994, **41**, 637 and refs. therein.
2 (*a*) F. Cecconi, C. A. Ghilardi and S. Midollini, *J. Chem. Soc., Chem. Commun.*, 1981, 640; (*b*) A. Agresti, M. Bacci, F. Cecconi, C. A. Ghilardi and S. Midollini, *Inorg. Chem.*, 1984, **24**, 689; (*c*) F. Cecconi, C. A. Ghilardi, S. Midollini, A. Orlandini and P. Zanello, *J. Chem. Soc., Dalton Trans.*, 1987, 831; (*d*) F. Cecconi, C. A. Ghilardi, S. Midollini, A. Orlandini and P. Zanello, *Polyhedron*, 1986, 2021; (*e*) D. Fenske, J. Ohmer and J. Hachgenei, *Angew. Chem., Int. Ed. Engl.*, 1985, **24**, 993; (*f*) D. Fenske, J. Ohmer, J. Hachgenei and K. Merzweiler, *Angew. Chem., Int. Ed. Engl.*, 1988, **27**, 1277; (*g*) T. Saito, N. Yamamoto, T. Yamagata and H. Imoto, *J. Am. Chem. Soc.*, 1988, **110**, 1646; (*h*) T. Saito, A. Yoshikawa, T. Yamagata, H. Imoto and K. Unoura, *Inorg. Chem.*, 1989, **28**, 3588; (*i*) T. Saito, N. Yamomoto, T. Nagase, T. Tsuboi, K. Kobayashi, T. Yamagata, H. Imoto and K. Unoura, *Inorg. Chem.*, 1990, **29**, 764; (*j*) M. L. Steigerwald, T. Siegrist and S. M. Stuczynski, *Inorg. Chem.*, 1991, **30**, 4945; (*k*) M. Hong, Z. Huang, X. Lei, G. Wei, B. Kang and H. Liu, *Polyhedron*, 1991, **10**, 927; (*l*) B. Hessen, T. Siegrist, T. Palstra, S. M. Tanzler and M. L. Steigerwald, *Inorg. Chem.*, 1993, **32**, 5165; (*m*) S. M. Stuczynski, Y.-U. Kwon and M. L. Steigerwald, *J. Organomet. Chem.*, 1993, **449**, 167.
3 R. Chevrel, M. Sergent and M. J. Prigent, *Mater. Res. Bull.*, 1974, **22**, 1487; A. Gruttner, K. Yvon, R. Chevrel, M. Potel, M. Sergent and B. Seeber, *Acta Crystallogr. Sect. B.*, 1979, **35**, 285.
4 (*a*) F. Cecconi, C. A. Ghilardi, S. Midollini and A. Orlandini, *Inorg. Chim. Acta*, 1991, **184**, 141; (*b*) J.-C. Gabriel, K. Boubekeur and P. Batail, *Inorg. Chem.*, 1994, **32**, 2894.
5 P. W. R. Corfield, R. J. Doedens and J. A. Ibers, *Inorg. Chem.*, 1967, **6**, 197.
6 N. Walker and D. Stuart, *Acta Crystallogr., Sect. A*, 1983, **39**, 158.
7 G. M. Sheldrick, SHELX 76 System of Computing Programs, University of Cambridge, 1976.
8 C. K. Johnson, ORTEP, Report ORNL-5138, Oak Ridge National Laboratory, Oak Ridge, TN, 1976.
9 *International Tables for X-Ray Crystallography*, Kynoch Press, Birmingham, 1974, vol. 4, p. 99.
10 R. F. Stewart, E. R. Davidson and W. T. Simpson, *J. Chem. Phys.*, 1965, **42**, 3175.
11 *International Tables for X-Ray Crystallography*, Kynoch Press, Birmingham, 1974, vol. 4, p. 149.
12 L. Casella, O. Carugo, M. Gullotti, S. Garofani and P. Zanello, *Inorg. Chem.*, 1993, **32**, 2056.
13 ADF, release 1.1.2, Department of Theoretical Chemistry, Vrije Universiteit, Amsterdam, 1994.
14 E. J. Baerends, D. E. Ellis and P. Ros, *Chem. Phys.*, 1973, **2**, 41.
15 G. te Velde and E. J. Baerends, *J. Comput. Phys.*, 1992, **99**, 84.
16 S. J. Volsko, L. Wilk and M. Nusair, *Can. J. Chem.*, 1980, **58**, 1200.
17 H. Stoll, E. Golka and H. Preuss, *Theor. Chim. Acta*, 1978, **49**, 143.
18 A. Bencini, F. Fabrizi de Biani and M. G. Uytterhoeven, *Inorg. Chim. Acta*, in the press.
19 W. H. Press, B. P. Flannery, S. A. Teukolsky and W. T. Vetterlig, *Numerical Recipes*, Cambridge University Press, Cambridge, 1989.
20 A. Bencini, S. Midollini and C. Zanchini, *Inorg. Chem.*, 1992, **31**, 2132.
21 R. Adams, T. S. Barnard, Z. Lee, W. Wu and J. Yamamoto, *Organometallics*, 1994, **13**, 2356; R. G. Teller, R. D. Wilson, R. K. McMullan, T. F. Koetzle and R. Bau, *J. Am. Chem. Soc.*, 1978, **100**, 3071; P. Braunstein, J. Rosé, D. Toussaint, S. Jaaskelainen, M. Ahlgren, T. A. Pakkanen, J. Pursiainen, L. Toupet and D. Grandjean, *Organometallics*, 1994, **13**, 2472 and refs. therein.
22 E. R. Brown and J. R. Sandifer, in *Physical Methods of Chemistry. Electrochemical Methods*, eds. B. W. Rossiter and J. F. Hamilton, Wiley, New York, 1986, vol. 2, ch. 4.
23 P. Zanello, in *Stereochemistry of Organometallic and Inorganic Compounds*, ed. P. Zanello, Elsevier, Amsterdam, 1994, vol. 5.
24 A. Bencini, C. A. Ghilardi, S. Midollini, A. Orlandini, U. Russo, M. G. Uytterhoeven and C. Zanchini, *J. Chem. Soc., Dalton Trans.*, 1995, 963.
25 A. Bencini, M. G. Uytterhoeven and C. Zanchini, *Int. J. Quantum Chem.*, 1994, **52**, 903.
26 N. Rosch, L. Ackermann and G. Pacchioni, *Inorg. Chem.*, 1993, **32**, 2963.

Received 4*th July* 1995; *Paper* 5/04332H